DOI 10.1007/s11182-022-02640-2
Russian Physics Journal, Vol. 65, No. 2, June, 2022 (Russian Original No. 2, February, 2022)

FINE STRUCTURE AND FRACTURE SURFACE OF LOW-CARBON STEEL WELDS

R. E. Kryukov,[1] V. E. Gromov,[1] Yu. F. Ivanov,[2] N. A. Kozyrev,[1] and Yu. A. Rubannikova[1]

UDC 620.170:621.791:669.018.29

Using the methods of modern physical materials science, the structural phase state, the defect substructure and the fracture surface of low-carbon alloy steel welds formed with and without carbon-containing additionы are studied. A quantitative analysis of the structure and dislocation substructure parameters of the weld metal is performed. The contributions from the scalar and excess dislocation density to the weld metal strength are estimated. It is noted that for a weld formed without any carbon-containing addition the level of internal stress fields is higher, which may result in the material embrittlement.

Keywords: dislocations, weld, fractography, structure, phase composition, fracture surface.

INTRODUCTION

Weld joints are essential elements of most structures. The structural-phase state, formed during welding and controlled by the welding modes and methods, affects the physical and mechanical characteristics of the resulting product. A challenging problem today is to improve the reliability of the metal structures operated in the northern territories. An important role in the solution of this problem belongs to welding fluxes and additives guaranteeing high physical-chemical properties of the weld joints. To select a proper chemical composition of the flux is a complex scientific-technical task.

The physical-mechanical properties of the welds depend not only on the metal weld composition but also on the content of nonmetallic inclusions present in it. Most nonmetallic inclusions found in the welds represent oxide compounds of exogenic and endogenic nature, which were formed as a result of metal deoxidation by silicon and manganese. In order to overcome this disadvantage it is necessary to use carbon-bearing fluxes or additives to them [1].

A reasonable selection of carbon-containing additives requires detailed studies of the structural-phase states of the welds by the methods of advanced physical materials science. The purpose of this work is to perform a comparative analysis of the structure and fracture surfaces of the welds formed with and without carbon-containing additives.

EXPERIMENTLA MATERIAL AND PROCEDURE

The elemental composition of the experimental weld metal samples is given in Table 1.

The submerged welding operations in the flux in the form of a slag of the silicomanganese production using a carbon additive in the amount of 6% (Sample No. 1) and without any additive (Sample No. 2) were performed without scarf-trimming neither side of the sample measuring 500×75 mm with a thickness of 16 mm, which was manufactured

[1]Siberian State Industrial University, Novokuznetsk, Russia, e-mail: rek_nzrmk@mail.ru; gromov@physics.sibsiu.ru; kozyrev_na@mtsp.sibsiu.ru; rubannikova96@mail.ru; [2]Institute of High Current Electronics of the Siberian Branch of the Russian Academy of Sciences, Tomsk, Russia, e-mail: yufi55@mail.ru.
Translated from Izvestiya Vysshikh Uchebnykh Zavedenii, Fizika, No. 2, pp. 126–130, February, 2022. Original article submitted July 12, 2021; revision submitted December 20, 2021.

TABLE 1. Chemical Compositions of the Weld Joint (rest – Fe, wt.%)

Sample	C	Si	Mn	Cr	Ni	Cu	Nb	Al	S	P
No. 1	0.12	0.66	1.43	0.02	0.06	0.10	0.011	0.012	0.027	0.008
No. 2	0.09	0.71	0.51	0.03	0.10	0.11	0.014	0.023	0.018	0.012

from the welding steel of the 09G2S (Russian State Standard 19281-2014) grade. The wire used in the welding process was Sv-08GA (Russian State Standard 2246-70) and the welding was carried out using an ASAW-1250 welding machine in the following modes: $I = 700$ A, $U = 30$ V, $V = 35$ m/h.

The sample dimensions and the weld joint type were consistent with the qualification requirements for the welding procedure and materials. The chemical composition of the FD-UFS carbon-containing additive according to TU 5929-007-01395874–2015 (wt.%) was the following: (21–46.23) Al_2O_3, (18–27) F, (8–15) Na_2O, (0.4–6.0) K_2O, (0.7–2.3) CaO, (0.5–2.48) SiO_2, (2.1– 3.27) Fe_2O_3, (12.5–30.2) C, (0.07–0.9) MnO, (0.06–0.9) MgO, (0.1–2.05) S, (0.1–0.18) P. The material consists of two-dimensionally ordered carbon ($d_0O_2 = 3.47$ Å, $L_c = 45.8$ Å), X-ray amorphous substance, cryolite, corundum, chiolite, and various impurities.

The chemical composition of the dump-slag flux (wt.%) was: (6.91–9.62) Al_2O_3, (22.85–31.70) CaO, (46.46–48.16) SiO_2, (0.27–0.81) FeO, (6.48–7.92) MgO, (8.01–8.43) MnO, (0.28–0.76) F, (0.26−0.36) Na_2O, ≤ 0.62 K_2O, (0.15–0.17) S, 0.01 P.

The structure of the fracture surface and that of the etched surface of the weld metal were analyzed by the methods of scanning electron microscopy. The sample surfaces were etched with a pulsed electron beam in the SOLO facility [2]. The irradiation parameters were the following: accelerated electron energy – 18 keV, electron beam power density – 10 J/cm^2, electron beam irradiation time – 50 μs, number of pulses – 3, pulse repetition frequency – 0.3 s^{-1}, irradiation was performed at a residual gas (argon) pressure of 0.02 Pa. The phase morphology, the defect substructure and the phase composition of the metal were examined by the methods of transmission electron diffraction microscopy (TEM) [3−5].

EXPERIMENTAL RESULTS AND DISCUSSION

According to Table 1, the weld samples differ in the degree of doping, specifically: the total concentration of the alloying elements (C, Si, Mn, Cr, Ni, Cu, Nb, Al) in Sample No. 1 was 2.413 wt.% and in Sample No. 2 – 1.487 wt.%. The main difference in the elemental compositions of metal welds of the experimental samples is observed in the contents of manganese and carbon.

The structural studies of etched weld sections revealed the presence of a large number of second-phase particles. An irradiation of the polished steel surface with a pulsed electron beam accompanied by a high-rate heating of the layer results in the formation of the second-phase precipitates (carbides, sulfides, oxides, etc.) and microcraters [6].

Figure 1 presents the results obtained in the studies of the fracture surface of the metal weld. Irrespective of the sample number, the fracture surface had been formed by the cleavage dimples. Frequently there are round second-phase particles on the bottom of the dimples (Fig. 1*b*, particles are indicated by the arrows). This evidences of the fact that the reason for material fracture is the presence of particles in this material volume [7]. The size of the dimples of ductile rupture in Sample No. 1 (Fig. 1*a*) is several times smaller compared with Sample No. 2 (Fig. 1*b*). The latter fact indicates a finer structure formed in the weld of Sample No. 1.

The fracture surfaces of the weld joints contain micropores irrespective of the sample number. The number of micropores on the fracture surface of Sample No. 1 is a few times larger compared to Sample No. 2, however, the micropore sizes in Sample No. 1 are a factor of 1.8 smaller than those in Sample No. 2.

Using the methods of transmission electron diffraction microscopy it has been revealed that the principal phase of the experimental welds, irrespective of the sample number, is α-iron solid solution. In addition to α-iron, the weld contains the particles of iron carbide (cementite) and, mainly in Sample No. 2, iron silicide (Fe_3Si with an fcc-lattice, $a = 0.28277$ nm).

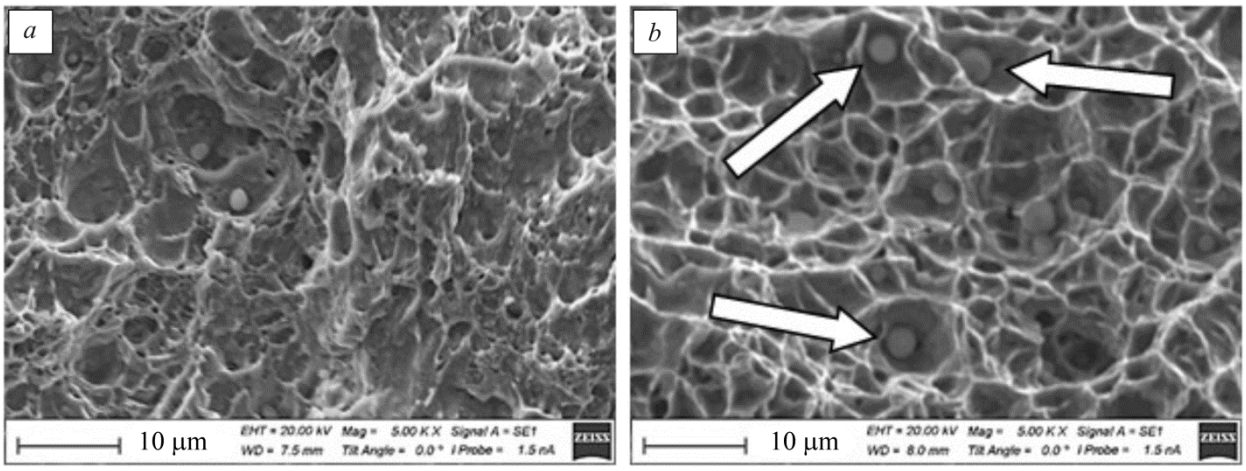

Fig. 1. Dimples of ductile fracture of the weld metal in Samples No. 1 (*a*) and No. 2 (*b*). Arrows in (*b*) indicate the second-phase particles.

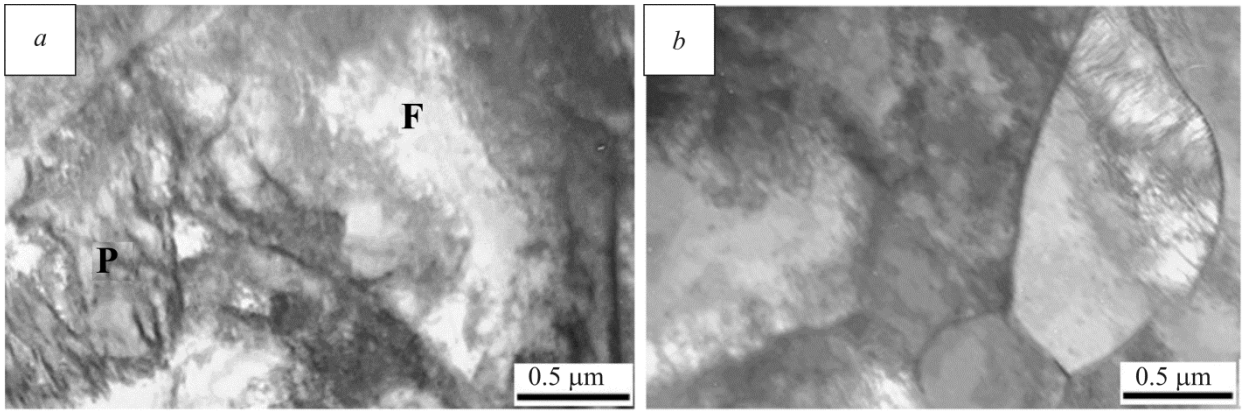

Fig. 2. TEM images of pearlite (*a*) and submicron ferrite (*b*) grains in the weld joint; in (*a*) P – pearlite grain, F – ferrite grain.

The dislocation structure observed in the bulk of the ferrite grains was classified in accordance with the data reported in [8, 9]. Firstly, there are regions with chaotically distributed dislocations. The scalar dislocation density, determined by the random intercept method, does not practically depend on the sample number and is found to be ~$3.58 \cdot 10^{10}$ cm^{-2}. Secondly, there are regions with cellular-network dislocation substructure. The scalar dislocation density in this structure in Sample No. 1 is $2.8 \cdot 10^{10}$ cm^{-2} and in Sample No. 2 – $3.5 \cdot 10^{10}$ cm^{-2}. A peculiar feature of the weld structure in Sample No. 2 is the presence of degenerated pearlite grains (Fig. 2*a*) and submicron ferrite grains (Fig. 2*б*). The content of pearlite grains is quite small; therefore their analysis in this work was omitted. The average ferrite grain size is 800 nm. The scalar density of chaotically distributed dislocations in the bulk of such grains is equal to $3.2 \cdot 10^{10}$ cm^{-2}.

An analysis of the weld structure by the method of thin foils allowed studying the internal stress fields revealed as the bending extinction contours [10] (Fig. 3). The studies have shown that the sources of the stress fields are the interphase interfaces (ferrate grain interfaces) phase boundaries (particle / matrix interfaces).

The electron microscopy examination of the welds allowed performing a quantitative analysis of the steel structure characteristics; the results are given in Table 2. We determined the scalar (ρ) and excessive ($\rho_{\pm}$) dislocation

TABLE 2. Analytical Data on Defect Substructure and Phase Composition of Welds

Structure parameters*	Sample No. 1	Sample No. 2
ρ, 10^{10}, cm^{-2}	2.92	3.22
$\rho_{\pm}$, 10^{10}, cm^{-2}	2.04	2.87
σ_f, MPa	340	360
σ_d, MPa	$285pl_{л} + 0_{els}$	$335_{pl}+130_{elas} = 465$
δ (Fe_3C)	0.97% (0.41% – at boundaries, 0.56% – in grain bulk)	0.30% (0.20% – at boundaries, 0.10% – in grain bulk)

Notations: * ρ – scalar dislocation density, ($\rho_{\pm}$) – excessive dislocation density σ_f – contribution into material hardening due to mobile dislocation drag by the forest dislocations, σ_d – contribution into material hardening due to internal stress fields (plastic and elastic deformation components), δ (Fe_3C) – volume fraction of cementite particles.

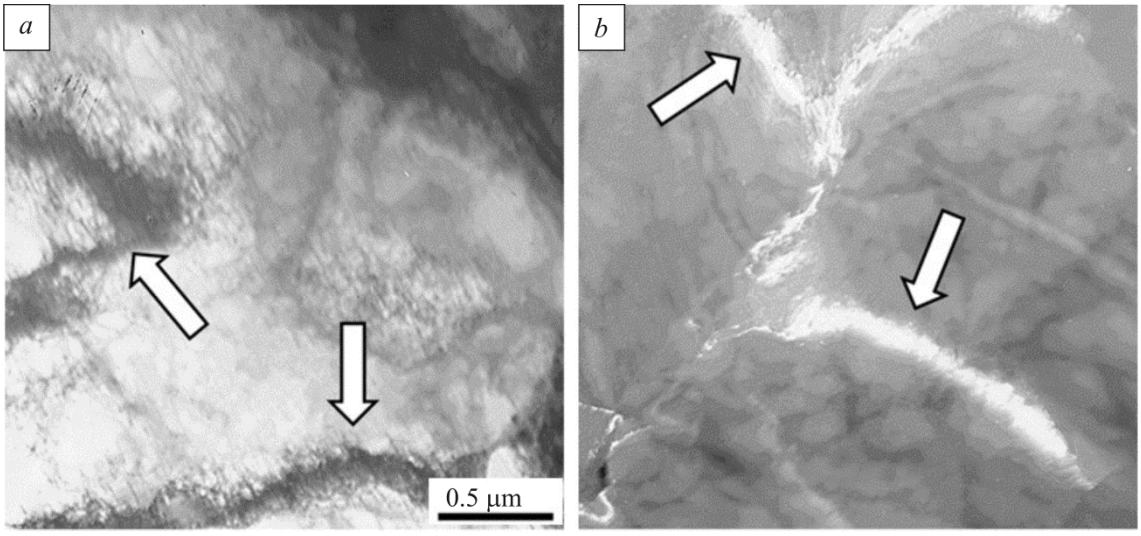

Fig. 3. TEM images of the bending extinction contours in the weld structure, *a* – bright-field image, *b* – тdark-field image in the [110]α-Fe reflection. The contours are indicated with arrows.

densities, the volume fraction of cementite (Fe_3C) and, using well-known relations [11], estimated the metal strengthening in the presence of the dislocation substructure and internal stress fields.

Analyzing the results listed in Table 2, one can note that the fraction of cementite in the weld structure of Sample No. 1 is larger than that in Sample No. 2, which seems to be due to a higher level of doping of the weld No. 1. The scalar and excessive dislocation densities in the metal structure of Sample 2 are higher than those in Sample No. 1. The higher scalar and excessive dislocation densities resulted in a larger contribution into the metal hardening due to the retarding of mobile dislocations by the forest dislocations (σ_f) and also the contribution into the metal hardening due to the internal stresses in Sample No. 2 compared to those of Sample No. 1. The latter circumstance suggests a higher level of internal stresses in the material of Sample No. 2 and, very likely, a higher number of stress concentrators that can cause material embrittlement in this sample.

CONCLUSIONS

Using the scanning electron microscopy and transmission electron microscopy diffraction, the structure, the phase composition, the dislocation substructure and the fracture surfaces of the weld joints of low-carbon steel

manufactured with (Sample No. 1) and without (Sample No. 2) a carbon-containing additive have been studied. The main phase of the weld joints is an α-Fe solid solution. The average ferrite grain size is ~800 nm. The dislocation substructure represents the chaotically distributed dislocation and the cellular-network substructure. It has been shown that the number of micropores on the fracture surface of Sample No. 1 is much larger than that in Sample No. 2, which could indicate degassing due to the use of a carbon-containing additive. It has been hypothesized that it is the higher values of the scalar and excessive dislocation densities in the weld joint formed without any welding additive in the flux which are responsible for the weld material embrittlement.

REFERENCES

1. N. A. Kozyrev, R. V. Kryukov, A. B. Poop, and U. I. Lipatova, Izvestiya VUZov. Chernaya Metallurg., **58**, No. 4, 258 (2015).
2. N. N. Koval and Yu. F. Ivanov, Structure Evolution of the Surface Layer of Steel Subjected to Electron-Ion-Plasma Treatment [in Russian], Publishing House of Scientific and Technology Literature, Tomsk (2016).
3. F. R. Egerton, Physical Principles of Electron Microscopy, Springer International Publishing, Basel (2016).
4. C. S.S. R. Kumar, Transmission Electron Microscopy. Characterization of Nanomaterials, Springer, N. Y. (2014).
5. C. B. Carter and D. B. Williams, Transmission Electron Microscopy, Springer International Publishing, Berlin (2016).
6. V. P. Rotstein, D. I. Proskurovsky, and G. Ye. Ozur, Modification of Surface Layers of Metallic Materials with Low-Energy High Current Electron Beams [in Ruasian], Nauka, Novosibirsk (2019).
7. Metals Handbook. Fractography and Atlas of Fractographs, American Society for Metals (1982).
8. E. V. Kozlov, A. N. Zhdanov, and N. A. Koneva, Physical Mesomechanics, **9**, No. 3-4, 75 (2006).
9. N. A. Koneva and E. V. Kozlov, Structural Levels of Plastic Deformation and Fracture (Ed. V. E. Panin) [in Russian], Nauka, Novosibirsk (1990).
10. G. Thomas and M. J. Goringe, Transmission Electron Microscopy of Materials, John Wiley and Sons, NY (1979).
11. A. A. Yuriev, V. E. Gromov, Yu. F. Ivanov, *et al*., Structure and Properties of Lengthy Rails after Extreme Long-Term Operation., Materials Research Forum LLC (2021).